Oxid Met (2012) 78:83–102
DOI 10.1007/s11085-012-9293-7

ORIGINAL PAPER

Alkali Induced High Temperature Corrosion of Stainless Steel: The Influence of NaCl, KCl and $CaCl_2$

S. Karlsson · J. Pettersson · L. -G. Johansson · J. -E. Svensson

Received: 8 July 2011 / Revised: 9 March 2012 / Published online: 27 April 2012

Abstract The influence of KCl, NaCl and $CaCl_2$ on the oxidation of 304-type (Fe18Cr10Ni) stainless steel at 600 °C in 5 $\%O_2$ + 40 $\%H_2O$ was investigated. Prior to exposure, a small amount of the preferred salt (cation equivalent: 1.35 μmol/cm^2) was deposited on the samples. Exposure time was 1–168 h. The oxidized samples were analyzed by SEM/EDX, XRD, FIB and IC. The presence of KCl and NaCl strongly accelerates high temperature corrosion of 304L. Corrosion attack is initiated by the formation of alkali chromate through the reaction of alkali with the protective oxide. Chromate formation is a sink for chromium in the oxide and leads to a loss of its protective properties. Subsequently a rapidly growing scale forms, consisting of an outer hematite layer with chromate particles on top and an inner spinel oxide layer. In contrast to NaCl and KCl, $CaCl_2$ is not very corrosive. At temperature, $CaCl_2$ is rapidly converted to CaO. Small amounts of $CaCrO_4$ form where CaO is in direct contact with the scale. CaO also reacts with the scale to form $Ca_2Fe_2O_5$.

Keywords Oxidation · Alkali · Breakaway corrosion · 304L · Chromate

S. Karlsson (✉) · J. Pettersson · L.-G. Johansson · J.-E. Svensson
Department of Chemical and Biological Engineering, Energy and Materials, Chalmers University of Technology, 412 96 Göteborg, Sweden
e-mail: sofia.karlsson@chalmers.se

J. Pettersson
e-mail: jpetter@chalmers.se

L.-G. Johansson
e-mail: lg@chalmers.se

J.-E. Svensson
e-mail: jes@chalmers.se

Introduction

The production of electricity from biomass and waste-fired power plants is increasing all over the world. Unfortunately, the combustion of biomass and waste results in the formation of corrosive deposits and gases. Besides water vapor and carbon dioxide, the flue gas contains high concentrations of alkali chlorides and hydrogen chloride while the sulphur dioxide content is typically low [1, 2]. Hence, the deposits formed on the superheater tubes are often rich in alkali chlorides which are known to cause accelerated corrosion of the superheater tubes [1–7]. The corrosivity of alkali chlorides in the presence of O_2 is often explained by applying "the chlorine cycle" mechanism [3, 5–10] where $Cl_2(g)$ plays a seminal role, acting as a catalyst for corrosion. Thus, the mechanism supposes that Cl_2 forms in a reaction between O_2 and alkali chloride at the scale/metal interface. Cl_2 then penetrates the scale and generates volatile transition metal chlorides at the scale/metal interface. The transition metal chlorides then diffuse back to the scale/gas interface where they are oxidized by O_2, precipitating metal oxide and releasing $Cl_2(g)$ which enters the process again.

Recently, a new, electrochemical, mechanism has been proposed to explain the alkali chloride-induced corrosion of low-alloyed steel. In the new mechanism, chloride ion is the diffusing chlorine species rather than Cl_2 [11]. Also, it has been reported recently that the potassium ion plays an important role in the initiation of KCl-induced corrosion of stainless steels [12–16]. Thus, it was shown that K_2CO_3 is equally corrosive as KCl towards stainless steel 304L at 600 °C. The corrosiveness of the potassium ion was attributed to the formation of potassium chromate(VI) by reaction with the oxide scale. The reaction depletes the oxide in chromium and destroys its protective properties [17].

The present study investigates the corrosion effects of three chloride salts (KCl, NaCl and $CaCl_2$) on the austenitic stainless steel 304L (Fe18Cr10Ni) in 5 %O_2 and 40 % H_2O at 600 °C. The emphasis is on the early stages of corrosion and on elucidating the sequence of events that cause the corrosion attack.

Experimental Procedures

Sample Preparation

The material investigated is the austenitic stainless steel, 304L, for chemical composition see Table 1. The geometrical area of the samples was 5.56 cm^2, ($15 \times 15 \times 2$ mm^3). For handling, a hole ($\varphi = 1.5$ mm) was drilled, 2 and 7.5 mm from the edges. Before exposure the samples were grinded on 320 grit SiC with

Table 1 Chemical composition of alloy 304L in wt%

	Fe	Cr	Ni	Mn	Si	Mo	N	C
304L	Balance	18.5	10.2	1.41	0.55	0.49	0.075	0.027

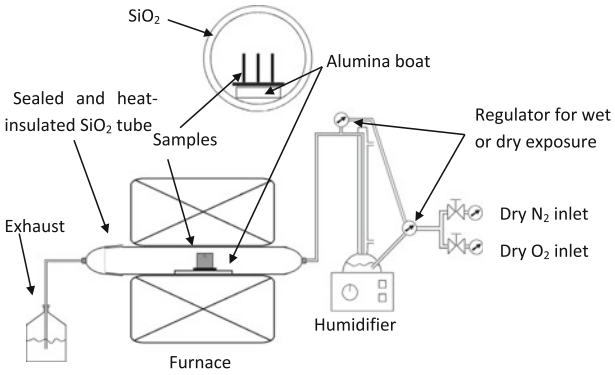

Fig. 1 Experimental setup for exposures in a horizontal silica tube furnace

deionized water. The samples were then polished with 9, 3 and 1 μm diamond solution and lubricating liquid on a polish cloth until a mirror-like surface appeared. After polishing, the samples were degreased and cleaned in acetone and ethanol using an ultrasonic bath. The samples were coated with the preferred salt (NaCl, KCl or $CaCl_2$) to a cation equivalent of 1.35 μmol/cm^2. The salts were applied by spraying the samples with a saturated solution of the prefer salt in water/ethanol. NaCl and KCl sprayed samples were weight in order to calibrate the amount. Because of the hygroscopic nature of $CaCl_2$, the amount was calibrated with ion chromatography. The samples were dried with air and stored in a desiccator prior to exposure. The mass change of the samples was measured prior to and after exposure using a six decimal Sartorius^{TM} balance.

Exposures

All exposures were isothermal and performed in silica tube furnaces with ex-situ recording of the weight (Fig. 1). The samples, three at time, were mounted on a sample holder and positioned parallel to the gas flow direction. The temperature was kept at 600 °C (±1 °C) and was calibrated before each exposure. The experiments were carried out in 5 %O_2 + 40 %H_2O and the flow rate was 2.5 cm/s. Nitrogen was used as carrier gas. The flow rate was controlled with a Bios DC2 Flow Calibrator. The dry gas was led through a humidifier and a temperature controlled condenser to obtain the correct water concentration. The experiments lasted 1, 24, 72 or 168 h.

Corrosion Product Characterization

X-ray Diffraction, XRD

The crystalline corrosion products were analysed with Grazing-Incidence X-Ray Diffraction (GI-XRD) using a Siemens D5000 powder diffractometer, equipped

with grazing—incidence beam attachment and a Göbel mirror. Cu K. ψ radiation was used and the angle of incidence was 2°–5°. The measurement range was $20° < 2\theta < 70°$.

Scanning Electron Microscopy, SEM/EDX

SEM imaging was performed using an FEI Quanta 200 ESEM FEG. The EDX detector is linked with the SEM and an Oxford Inca EDX system was used. The microscope was operated at 15–20 kV.

Ion Chromatography, IC

To determine the amount of water-soluble anions (Cl^- and CrO_4^{2-}) a Dionex ICS-90 system was used. The anions were analysed with an IonPac AS4A-SC analytic column and 1.8 mM Na_2CO_3/1.7 mM $NaHCO_3$ was used as eluent. To determine the amount of water-soluble cations (K^+, Na^+ and Ca^{2+}) a Dionex ICS-900 system was used. The anions were analysed with an IonPac CS12A analytic column and 20 mM sulfonic acid was used as eluent. The flow rate was 2 mL/min for both anions and cations analyses.

Results

Gravimetry

Figure 2 shows mass gain as a function of exposure time for 304L steel in 5 %O_2 + 40 %H_2O environment at 600 °C in the presence of NaCl, KCl and $CaCl_2$. The graph includes a reference exposure performed in the absence of salt. The results show that both NaCl and KCl strongly accelerate corrosion. While the

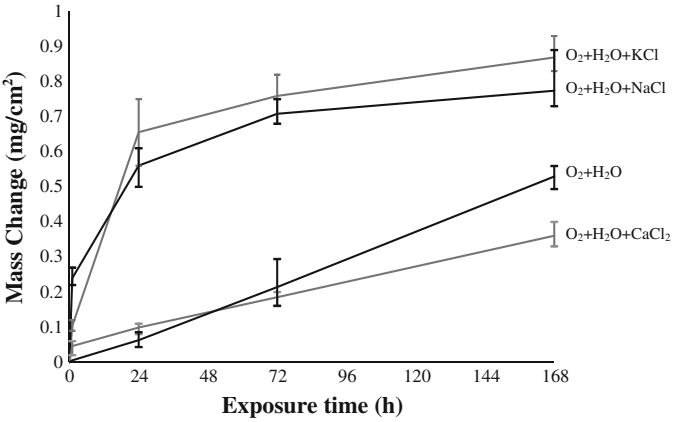

Fig. 2 Mass gain versus exposure time for samples exposed in the presence of NaCl, KCl, $CaCl_2$ in 5 %O_2 + 40 %H_2O at 600 °C. Reference exposures in 40 %H_2O at 600 °C are also included

two mass gain curves are similar during later stages of the exposures, NaCl initially causes higher mass gain than KCl. In contrast, exposure in the presence of $CaCl_2$ does not result in a significantly increased mass gain.

Surface Morphology

The surface morphology was investigated by Scanning Electron Microscope (SEM). Figure 3 shows plan view images after 1 and 24 h of exposure in the presence and in the absence of salt. Figure 3a shows a SEM image of a reference sample exposed for 1 h in $O_2 + H_2O$ at 600 °C. The environment results in the formation of large iron-rich oxide island on the surface. Similar oxide islands were observed in

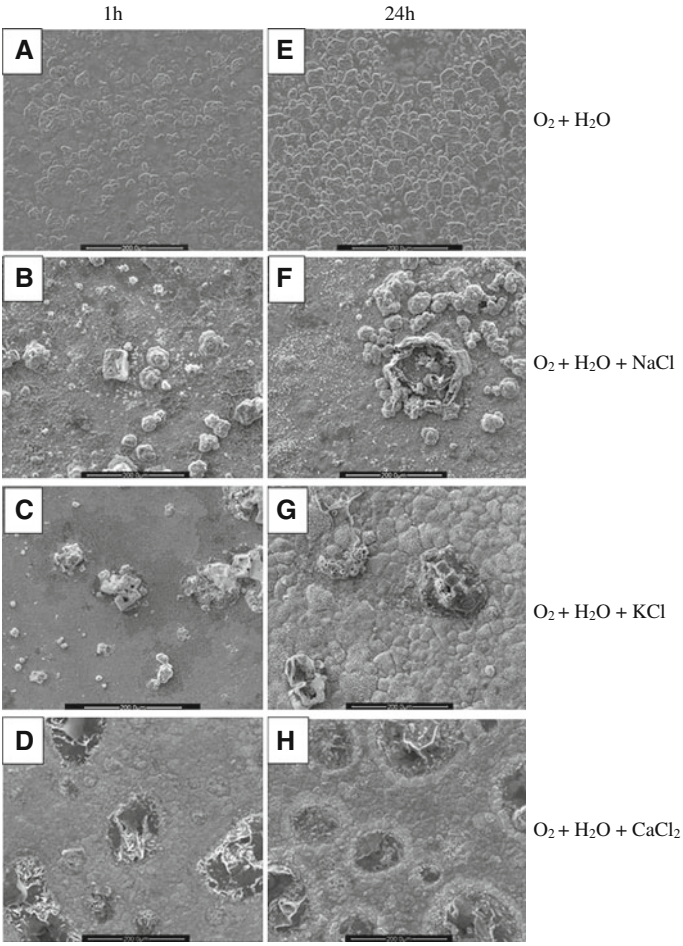

Fig. 3 SEM images of samples exposed for 1 and 24 h at 600 °C in **a** and **e**: 5 $\%O_2 + 40\ \%H_2O$, **b** and **f**: 5 $\%O_2 + 40\ \%H_2O + NaCl$, **c** and **g**: 5 $\%O_2 + 40\ \%H_2O + KCl$, **d** and **h**: 5 $\%O_2 + 40\ \%H_2O + CaCl_2$

previous investigations of the oxidation of 304L in $O_2 + H_2O$ environment at 600 °C. The earlier studies show that the oxide islands have formed in the middle of the underlying steel grains while the areas close to the steel boundaries remain protective. Figure 3b and c show samples exposed for 1 h in the presence of NaCl and KCl, respectively. In both cases, the salt particles are partly reacted and have started to become overgrown by oxide. At this stage the NaCl treated sample exhibit considerably more corrosion between the salt particles than in the case of KCl. Figure 3d shows a sample exposed for 1 h in the presence of $CaCl_2$. The salt agglomerates have a roughly circular form and at this stage $CaCl_2$ is partially decomposed (see XRD and IC analysis below). The surface between the salt agglomerations is relatively even. Oxide islands have started to form, similar to the ones observed in the reference run (compare Fig. 3a). Furthermore, there is no tendency for the salt agglomerations to become overgrown by oxide.

Figure 3e shows the surface after 24 h exposure in the absence of salt (reference sample). The oxide islands have increased both in number and size while the areas near the steel borders remain protective. Figure 3f and g show samples after 24 h exposure in the presence of NaCl and KCl, respectively. At this stage the surface is covered by thick scale, the former salt crystals being replaced by irregularly shaped oxide agglomerations. The surface between the oxide agglomerations is very uneven. The KCl treated samples exhibits an island-like scale morphology that reflects the substrate grain structure. In the case of NaCl, the corrosion affects the entire surface and no preferential corrosion of the grain centers is observed.

Figure 3h shows a sample after 24 h of exposure in the presence $CaCl_2$, showing roughly circular areas corresponding to the deposited salt. Between the circular formations, the oxidation morphology resembles the reference sample (see Fig. 3e), showing oxide islands. In the position of the former $CaCl_2$ agglomerations the scale tends to spall, see Fig. 4 for 45° tilted SEM image.

Increasing the exposure time from 24 to 168 h only produced minor changes in corrosion morphology.

Corrosion Product Characterization

The surface of the exposed samples was investigated with respect to elemental distribution and crystalline corrosion products using SEM/EDX together with XRD. EDX analyses (not shown) reveal that much of the NaCl and KCl added remains unreacted after 1 h at 600 °C. Accordingly, XRD (Figs. 5, 6) features strong diffraction peak from the salts. The crystalline corrosion products identified after 1 h of exposure were hematite (Fe_2O_3), spinel type oxide (Me_3O_4) and alkali chromate (Na_2CrO_4 or K_2CrO_4) indicating that the protective oxide has started to be converted to a poorly protective iron-rich oxide. However, strong diffraction from the steel substrate indicates that much of the surface is still covered by very thin oxide.

In contrast to the behavior of NaCl and KCl, the EDX analyses shows that $CaCl_2$ has largely decomposed after 1 h, the former $CaCl_2$ agglomerates exhibiting just a few percent of chlorine (not shown). XRD (Fig. 7) shows no evidence for $CaCl_2$ or its hydrates. There was very weak diffraction from CaO and the corrosion product

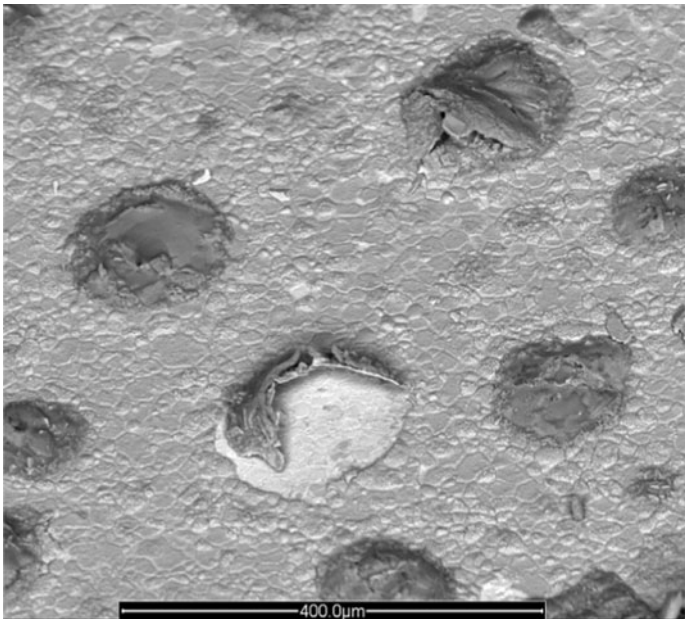

Fig. 4 45° tilted SEM image showing spallation of a former $CaCl_2$ salt crystal on the sample exposed for 24 h in the presence of $CaCl_2$ at 600 °C in 5 $\%O_2$ + 40 $\%H_2O$

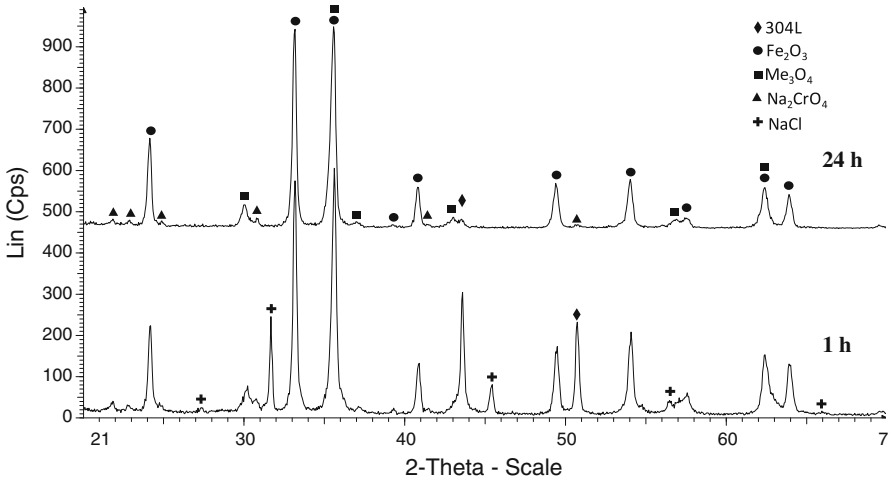

Fig. 5 Combined diffractogram for 304L samples exposed in 5 $\%O_2$ + 40 $\%H_2O$ + NaCl at 600 °C after 1 and 24 h. The upper diffractogram shows the sample exposed for 24 h and the under diffractogram shows the sample exposed for 1 h. The matching peaks in both diffractogram are marked in the upper diffractogram. The peaks that are only presence after 1 h are marked in the under one

detected were Fe_2O_3, spinel type oxide (Me_3O_4) and small amounts of dicalcium ferrate (III), $Ca_2Fe_2O_5$. Also in this case there was strong diffraction from the steel indicating the presence of a very thin oxide scale.

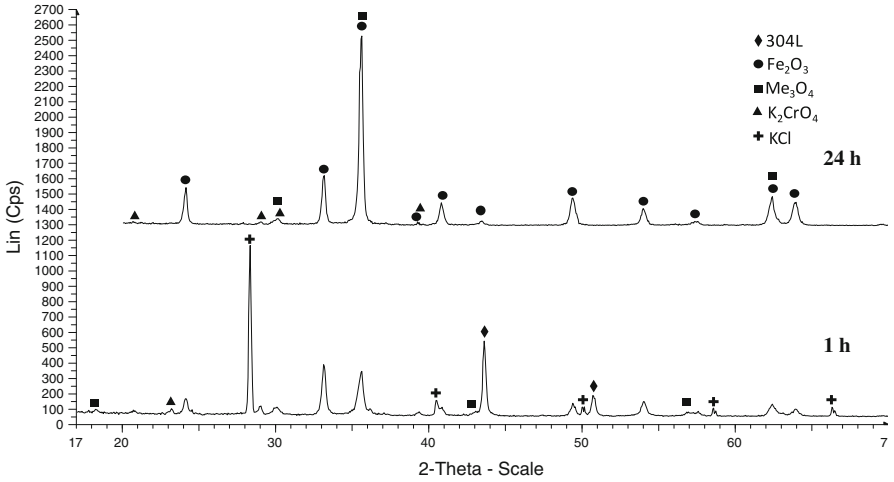

Fig. 6 Combined diffractogram for 304L samples exposed in 5 $\%O_2$ + 40 $\%H_2O$ + KCl at 600 °C after 1 and 24 h. The upper diffractogram shows the sample exposed for 24 h and the under diffractogram shows the sample exposed for 1 h. The matching peaks in both diffractogram are marked in the upper diffractogram. The peaks that are only presence after 1 h are marked in the under one

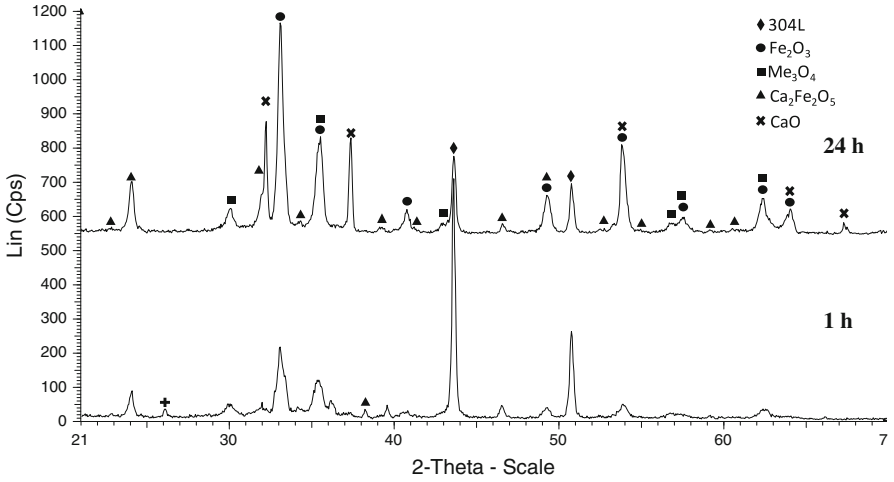

Fig. 7 Combined diffractogram for 304L samples exposed in 5 $\%O_2$ + 40 $\%H_2O$ + $CaCl_2$ at 600 °C after 1 and 24 h. The upper diffractogram shows the sample exposed for 24 h and the under diffractogram shows the sample exposed for 1 h. The matching peaks in both diffractogram are marked in the upper diffractogram. The peaks that are only presence after 1 h are marked in the under one

The fact that only small amounts of crystalline calcium-containing substances ($Ca_2Fe_2O_5$ and CaO) were identified implies that other, non-crystalline or poorly crystalline, calcium containing compounds is present at this stage. It is proposed that these compounds are products of the thermal decomposition of $CaCl_2$, consisting of hydroxy-chlorides (e.g., Ca(OH)Cl) or oxy-chlorides (e.g., Ca_2OCl_2) [18].

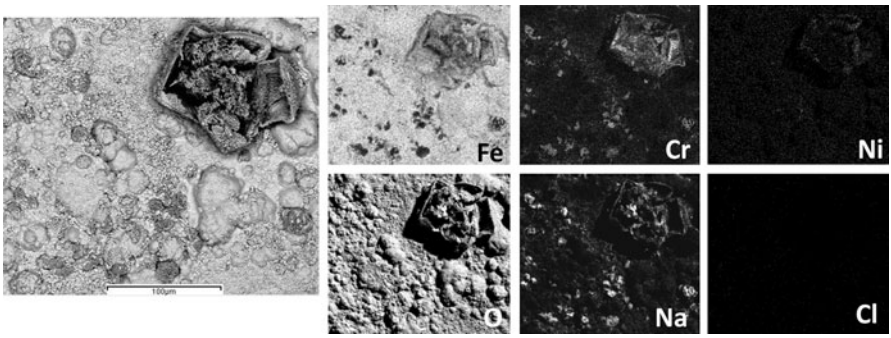

Fig. 8 EDX images of a sample exposed for 24 h in presence of NaCl at 600 °C in 5 $\%O_2$ + 40 $\%H_2O$

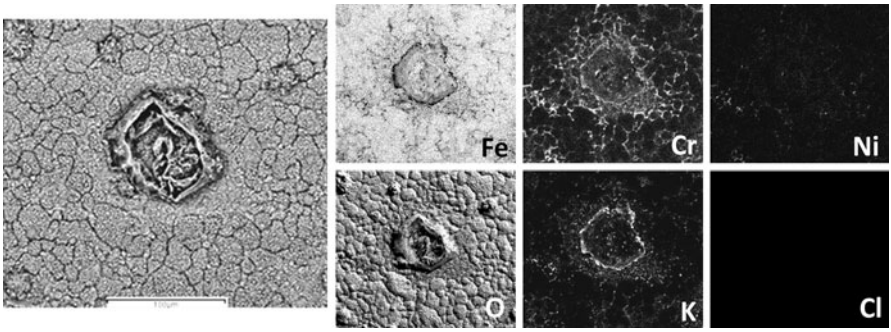

Fig. 9 EDX images of a sample exposed for 24 h in presence of KCl at 600 °C in 5 $\%O_2$ + 40 $\%H_2O$

Figures 8 and 9 show the surface after 24 h exposure in the presence of NaCl and KCl, respectively. In both cases, the surface is covered by iron-rich oxide. While the XRD results (Figs. 5, 6) show the same corrosion products as after 1 h, there is no diffraction from KCl or NaCl at this stage, indicating that the salts have reacted completely and/or evaporated. There is no or very weak diffraction from the steel substrate which indicates that most of the surface is covered by a thick oxide scale. Morphological features reminiscent of the original salt particles and consisting of corrosion product agglomerations are present on the surface. Areas rich in sodium and potassium are found in and between these features. Both elements are correlated to chromium and oxygen in the EDX maps. Sodium chromate (Na_2CrO_4) and potassium chromate (K_2CrO_4) were identified by XRD on the NaCl- and KCl-treated samples, respectively. Hence, the Na- and K-rich areas are attributed to sodium chromate and potassium chromate. In addition, EDX point analyses of NaCl treated samples (not shown) reveal that the amount of Na detected exceeds the amount of chromate in some areas. Furthermore, EDX and XRD analysis gave no evidence for transition metal chlorides.

After 24 h exposure in the presence of $CaCl_2$, the corrosion morphology is very different from that of the NaCl and KCl treated samples, see Fig. 10. In this case

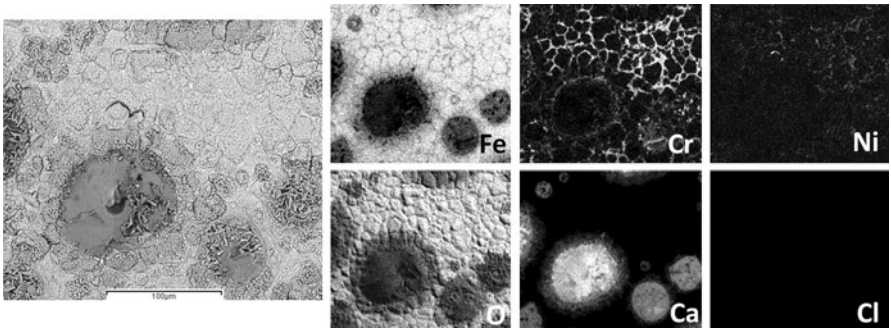

Fig. 10 EDX images of a sample exposed for 24 h in presence of $CaCl_2$ at 600 °C in 5 $\%O_2$ + 40 $\%H_2O$

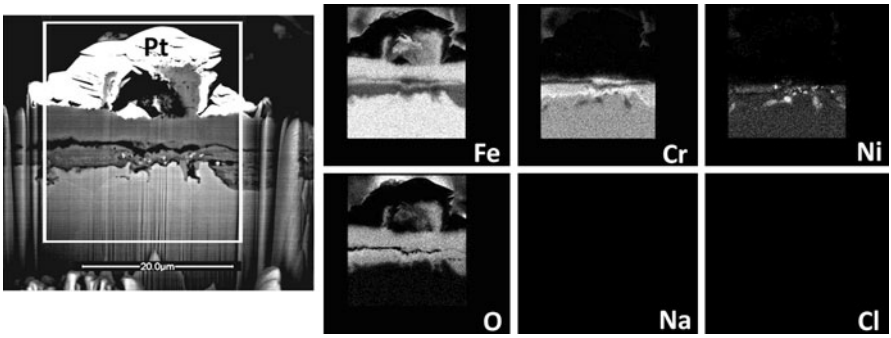

Fig. 11 EDX images of a FIB cross section through a former salt crystal on a sample exposed for 24 h in presence of NaCl at 600 °C in 5 $\%O_2$ + 40 $\%H_2O$

there are no corrosion product agglomerations. The area between the original salt particles is partly covered by thin, iron-rich oxide islands. The image shows a network pattern consisting of thin oxide scale, corresponding to the grain boundaries in the steel substrate. The presence of thin oxide is in accordance with the detection of strong X-ray diffraction from the steel substrate (see Fig. 7). EDX indicated that there is no Ca in this area. XRD shows very strong diffraction from CaO and relatively strong diffraction from $Ca_2Fe_2O_5$ at this stage. This implies that the decomposition of calcium chloride is now complete. EDX mapping shows that CaO forms patches that correspond to the original agglomerations of $CaCl_2$ particles (compare also Fig. 3h). $Ca_2Fe_2O_5$ is located in the periphery of the CaO patches. CaO is absent in some of the smaller circular areas, implying that it has been consumed by reaction with the scale, forming $Ca_2Fe_2O_5$. The overlap between Ca and Cr at the edges of the circular patches indicates the presence of $CaCrO_4$.

In order to further investigate the oxide scale, FIB cross sections were prepared from samples exposed for 24 h in the presence of salt, see Figs. 11, 12, and 13. In the case of NaCl and KCl, the FIB cross sections were prepared through a former salt particle. In the case of $CaCl_2$, the FIB cross section was performed at the edge of the former $CaCl_2$ agglomerates including both the area originally covered by salt

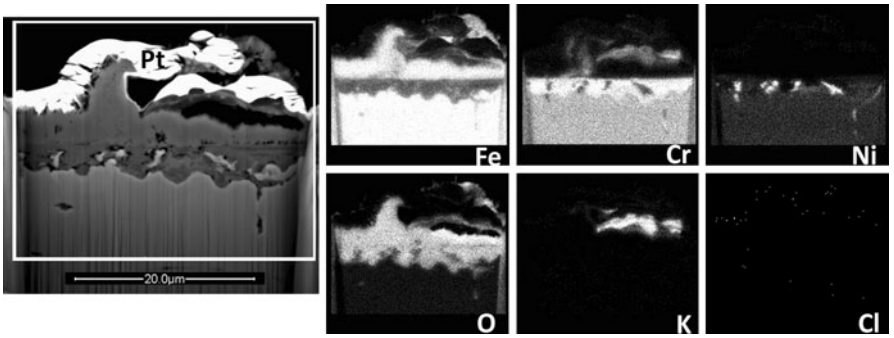

Fig. 12 EDX images of a FIB cross section through a former salt crystal on a sample exposed for 24 h in presence of KCl at 600 °C in 5 $\%O_2$ + 40 $\%H_2O$

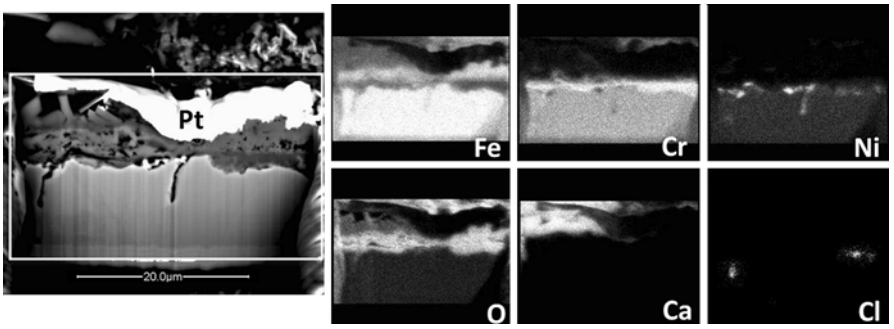

Fig. 13 45° tilted EDX images of a FIB cross section partly through a former salt crystal on a sample exposed for 24 h in presence of $CaCl_2$ at 600 °C in 5 $\%O_2$ + 40 $\%H_2O$

and the surrounding area. A platinum layer was first deposited on the selected area in order to protect the oxide.

Figure 11 shows a FIB cross section prepared through a former NaCl crystal after 24 h exposure at 600 °C. The shape of the former NaCl crystal can still be discerned but neither Na nor Cl is detected within its shape. A thick layered oxide scale has formed beneath the former NaCl crystal. The upper part of the scale consists of almost pure iron oxide while the bottom part shows high concentrations of chromium, iron and nickel. While iron and chromium are evenly distributed in the bottom part of the scale the nickel distribution is more uneven. Local enrichments of metallic nickel are also present in the alloy substrate immediately below the scale. No chlorine was detected. Based on this information and on the evidence from XRD (see Fig. 5) it is concluded that the upper iron-rich oxide corresponds to hematite while the bottom part of the scale is made up of spinel type oxide.

Figure 12 shows a corresponding sample exposed in presence of KCl. The corrosion morphology is similar to the NaCl case. Thus, a two layered oxide scale has formed beneath the former salt particle, consisting of an outer iron-rich layer and an inner layer containing iron, chromium and nickel. Again, the distribution of Ni in the bottom part of the scale is very uneven. In this case the oxygen map

implies that at least some of the Ni in the lower part of the scale is metallic. An area rich in potassium, chromium and oxygen is detected within the former salt particle. Based on XRD (see Fig. 6) and EDX point analysis it is concluded that this is potassium chromate (K_2CrO_4). Again, no chlorine was detected.

Figure 13 shows a sample exposed for 24 h in presence of $CaCl_2$. The FIB cross section includes part of the former $CaCl_2$ agglomerate and the surrounding area. The metal not covered by $CaCl_2$ has formed a two-layered oxide scale consisting of an iron oxide top layer and a bottom layer containing oxygen, iron, chromium and nickel. Again, it is suggested that the top and bottom parts are made up of hematite and spinel oxide respectively, both phases being detected by XRD. The area formerly covered by $CaCl_2$ exhibits a scale consisting of three distinctive layers. The outer part is rich in iron and calcium, the middle part is iron-rich together with small amounts of chromium while the bottom part contains iron, chromium and nickel. The combination of SEM/EDX and the XRD analysis (see Fig. 7) allows us to attribute the upper iron-calcium-rich oxide to dicalcium ferrate(III) ($Ca_2Fe_2O_5$). Similarly, it is considered that the middle, iron-rich oxide most consists of hematite while the bottom part of the scale is made up of spinel type oxide. As in the case of NaCl and KCl treated samples, nickel is unevenly distributed in the scale while there is an even distribution of chromium and iron. According to the EDX analysis of the FIB cross section, some areas at the metal/oxide interface contain chlorine and no calcium. These areas are suggested to contain transition metal chlorides although no such compounds were detected by XRD.

Analysis of Water Soluble Compounds

Tables 2, 3, 4 show the results from the ion chromatography (IC) analysis of the salt treated samples after 1, 24 and 168 h exposure. Tables 2 and 3 show the results for the samples exposed in the presence NaCl and KCl. After 1 h of exposure, the results are similar for the two salts. About 80 % of the applied alkali and about 60 % of the added chlorine is detected. The discrepancy between the amounts of alkali and chlorine found is attributed to the formation of alkali chromate with the simultaneous release of HCl(g) (see "Discussion" section).

After 24 h of exposure 44 % of the applied Na^+ was retrieved while the corresponding value for K^+ was only 19 %. Very little chlorine remained on the two samples. In the case of KCl the amount of potassium ions found after 24 h corresponds to the amount of chromate detected. In contrast, after 24 h the amount of sodium ions found on the NaCl treated samples exceeds the amount of chromate. After 168 h the NaCl treated samples showed essentially the same amounts of soluble ions as after 24 h. In contrast, the KCl treated samples show a decrease in the amount of chromate and of potassium from 24 to 168 h of exposure.

Table 4 shows the IC analysis of the samples exposed in the presence $CaCl_2$. After 1 h of exposure 52 % of the applied Ca^{2+} was detected. There is a strong decrease in the amount of chloride ions (12 % of the added amount being detected) which is attributed to the thermal decomposition and reaction of $CaCl_2$, forming CaO, $Ca_2Fe_2O_5$ and HCl(g). A small amount of CrO_4^{2-} has formed, corresponding to 2 % of the theoretical yield of $CaCrO_4$. After 24 h the amount of chromate has increased

Table 2 Water soluble ions by ion chromatography after 1, 24 and 168 h exposure at 600 °C in 5 %O_2 + 40 %H_2O in the presence of NaCl

	1 h	24 h	168 h
Fraction of Cl^- remaining	65 %	4 %	3 %
Fraction of Na^+ remaining	79 %	44 %	48 %
Chromate (CrO_4^{2-}) formation, (percent of theoretical yield)	16 %	30 %	33 %
Fraction of added Na^+ not accounted for[a]	21 %	56 %	52 %
Fraction of added Cl^- not accounted for[a]	19 %	66 %	64 %
Suggested molar balance for added NaCl	64 % NaCl, 16 % Na_2CrO_4, 20 % lost as NaCl(g)	4 % NaCl, 30 % Na_2CrO_4, 10 % "$Na_2Fe_2O_4$", 56 % lost as NaCl(g)	3 % NaCl, 33 % Na_2CrO_4, 12 % "$Na_2Fe_2O_4$", 52 % lost as NaCl(g)

1.35 μmol Na^+/cm^2 was added per sample. The amount of ions found is expressed as the percentage remaining of the amount added or (for CrO_4^{2-}) in percent of the theoretical yield

[a] The NaCl not accounted for by the IC analysis is attributed to vaporization of NaCl. Small amounts of NaCl may also be lost during handling. The relative standard deviation of the analysis corresponds to about ±5 %

Table 3 Water soluble ions by ion chromatography after 1, 24 and 168 h exposure at 600 °C in 5 %O_2 + 40 %H_2O in the presence of KCl

	1 h	24 h	168 h
Fraction of Cl^- remaining	59 %	2 %	2 %
Fraction of K^+ remaining	78 %	19 %	12 %
Chromate (CrO_4^{2-}) formation, (percent of theoretical yield)	18 %	20 %	11 %
Fraction of added K^+ not accounted for[a]	22 %	81 %	88 %
Fraction of added Cl^- not accounted for[a]	42 %	78 %	87 %
Suggested approximate molar balance for added KCl	60 % KCl, 18 % K_2CrO_4, 22 % lost as KCl(g)	2 % KCl, 18 % K_2CrO_4, 80 % lost as KCl(g)	1 % KCl, 11 % K_2CrO_4, 88 % lost as KCl(g) and by decomposition of K_2CrO_4

1.35 μmol of K^+ was added per sample. The amount of ions found is expressed as the percentage remaining of the amount added or (for CrO_4^{2-}) in percent of the theoretical yield

[a] The KCl not accounted for by the IC analysis is attributed to vaporization of KCl. Small amounts of KCl may also be lost during handling. The relative standard deviation of the analysis corresponds to about ±5 %

slightly but is still just a few percent of the theoretical yield. It is suggested that $CaCl_2$ has decomposed completely at this stage. Thus, the small amount of chlorine found is

Table 4 Water soluble ions by ion chromatography after 1, 24 and 168 h exposure at 600 °C in 5 %O_2 + 40 %H_2O in the presence of $CaCl_2$

	1 h	24 h	168 h
Fraction of Cl^- remaining	12 %	2 %	1 %
Fraction of soluble Ca^{2+} remaining	52 %	44 %	43 %
Chromate (CrO_4^{2-}) formation, (percent of theoretical yield)	2 %	4 %	5 %
Fraction of added Ca^{2+} not accounted for[a]	48 %	56 %	57 %
Fraction of added Cl^- not accounted for[b]	88 %	98 %	99 %
Suggested molar balance for Ca^{2+}	2 % $CaCrO_4$, 50 % as partially decomposed $CaCl_2$ and CaO, 48 % $Ca_2Fe_2O_5$ and lost by spallation	4 % $CaCrO_4$, 39 % CaO, 56 % $Ca_2Fe_2O_5$ and lost by spallation	5 % $CaCrO_4$, 38 % CaO and 57 % $Ca_2Fe_2O_5$ and lost by spallation
Suggested molar balance for Cl^-	12 % present as partially dec. $CaCl_2$, 88 % lost as HCl(g) by th.dec. of $CaCl_2$	2 % present as $FeCl_2$, 98 % lost as HCl(g) by th.dec. of $CaCl_2$	1 % present as $FeCl_2$, 99 % lost as HCl(g) by th.dec. of $CaCl_2$

1.35 μmol Ca^{2+}/cm^2 was added per sample. The amount of ions found is expressed as the percentage remaining of the amount added or (for CrO_4^{2-}) in percent of the theoretical yield

The relative standard deviation of the analysis corresponds to about ±5 %

[a] The Ca^{2+} not accounted for by IC is attributed mainly to formation of $Ca_2Fe_2O_5$. There were also substantial losses by scale spallation

[b] The chloride not accounted for by IC is attributed mainly to thermal dec. of $CaCl_2$

attributed to the transition metal chlorides detected by SEM/EDX (see Fig. 13). Extending the exposure time to 168 h does not change the results appreciably.

Discussion

Previous studies show that 304L initially forms a smooth, thin (<200 nm) Cr-rich $(Fe,Cr)_2O_3$ protective scale in dry O_2 at 600 °C [19–21]. In the presence of water vapor chromium is volatilized by formation of $CrO_2(OH)_2$ on the oxide surface [19, 20, 22]:

$$\begin{aligned} &Cr_2O_3(s) + 2H_2O(g) + 1.5O_2(g) \rightleftarrows 2CrO_2(OH)_2(g) \\ &\Delta G = 105\,\mathrm{kJ/mol}, \quad p_{eq}(CrO_2(OH)_2) \\ &\quad = 0.02 \times 10^{-6}\,\mathrm{bar\ at\ 600\,^{\circ}C, 5\,\%O_2, 40\,\%H_2O} \end{aligned} \tag{1}$$

Chromium volatilization depletes the protective oxide and the steel substrate in chromium. If the chromium content drops below a critical level the oxide loses its protective properties and an iron-rich, rapidly growing oxide forms. Therefore, the supply of chromium to the oxide by diffusion in the metal must match the

evaporation rate to maintain the protective properties of the oxide. At the alloy grain boundaries the diffusion is higher compared to the center of the steel grains. Hence, the oxidation behavior of the steel surface depends on the distance to a grain boundary. This explains why "islands" consisting of thick oxide form on central parts of the underlying steel grains while the areas close to a grain boundary retain a thin slow-growing oxide (see Fig. 3a, e). The oxide islands consist of an outer hematite (Fe_2O_3) and inner spinel-type ($(Fe, Cr, Ni)_3O_4$) layer [23].

In general, any process that depletes the protective oxide and the steel substrate in chromium is expected to make the stainless steel more vulnerable to high temperature corrosion. The present study explores chromate formation as a mechanism for chromium depletion, showing that both NaCl or KCl can trigger a breakdown of the protective oxide on 304L by formation of Na_2CrO_4 and K_2CrO_4, respectively (see Figs. 5, 6, 8, 9 and Tables 2, 3) [24]:

$$\begin{aligned} &Cr_2O_3(s) + 4NaCl(s) + 2H_2O(g) + {}^3\!/_2 O_2(g) \rightleftarrows 2Na_2CrO_4(s) + 4HCl(g) \\ &\Delta G = 163\,\mathrm{kJ/mol}, \quad p_{eq}(HCl) = 740 \times 10^{-6}\,\mathrm{bar\ at\ 600\,^\circ C}, 5\,\%O_2, 40\,\%H_2O \end{aligned} \tag{2}$$

$$\begin{aligned} &Cr_2O_3(s) + 4KCl(s) + 2H_2O(g) + {}^3\!/_2 O_2(g) \rightleftarrows 2K_2CrO_4(s) + 4HCl(g) \\ &\Delta G = 147\,\mathrm{kJ/mol}, \quad p_{eq}(HCl) = 1303 \times 10^{-6}\,\mathrm{bar\ at\ 600\,^\circ C}, 5\,\%O_2, 40\,\%H_2O \end{aligned} \tag{3}$$

The results show that chromate formation starts during the first exposure hour. After 24 h, chromates can be detected all over the surface which indicates that both KCl and NaCl diffuses out from the salt particle and react with the protective oxide that initially forms. It is proposed that chromium depletion of the protective oxide by reactions (2) and (3) result in a breakdown of the protective properties of the oxide, triggering the formation of a rapidly growing iron-rich scale. This is in accordance with earlier reports on the influence of KCl on the high temperature corrosion of 304L [12–14]. The resulting thick scale consists of an outer hematite layer and an underlying (Fe, Cr, Ni) spinel type oxide (see Figs. 11, 12) [16]. It is expected that this two-layered scale is poorly protective and the formation appears to be much faster compared to the breakdown triggered by chromium oxide hydroxide volatilization in the absence of salt.

As shown in Tables 2 and 3, about 60 % of the salts is still unreacted after 1 h. Furthermore, considerable amounts of alkali chromate have formed already during this first hour. However, about 20 % of the salts are not accounted for by the IC analysis and it is suggested that this is because of vaporization of the salts. The equilibrium partial pressure of NaCl and KCl at 600 °C are 1.4×10^{-6} bar and 3.3×10^{-6} bar, respectively [24]. The results show that chromate formation and volatilization of the salt continues during the first 24 h. It may be noted that the amount of chromate on the surface is similar after 24 and 168 h in the case of NaCl. In contrast, the amount of chromate decreases significantly with time in the case of KCl, suggesting that K_2CrO_4 tends to decompose. The decomposition of potassium chromate by reaction with water is not thermodynamically favoured: permeable for oxide and chloride ions. Thus, the scale structure is similar to the oxide islands

formed on 304L in $O_2 + H_2O$ environment in the absence of salt. The destruction of the protective scale by chromate [24]

$$\begin{aligned} &K_2CrO_4(s) + 2H_2O(g) \rightleftarrows 2KOH(l) + CrO_2(OH)_2(g) \\ &\Delta G = 348\,\text{kJ/mol}, \quad p_{eq}(CrO_2(OH)_2) = 8 \times 10^{-23}\,\text{bar at } 600\,^{\circ}\text{C}, 40\,\%H_2O \end{aligned} \tag{4}$$

Decomposition to Cr_2O_3 by water is also not favoured [24]:

$$\begin{aligned} &K_2CrO_4(s) + H_2O(g) \rightleftarrows 2KOH(l) + {}^1\!/_2Cr_2O_3(s) + {}^3\!/_4O_2(g) \\ &\Delta G = 231\,\text{kJ/mol, at } 600\,^{\circ}\text{C}, 40\,\%H_2O \end{aligned} \tag{5}$$

Instead, it is argued that potassium chromate decomposes electrochemically. The oxidation of metals in oxygen gas at high temperature is usually described in terms of a mechanism where molecular oxygen is reduced on the scale surface while metal is being oxidized at the scale/metal interface, the two reactions being coupled by electronic and ionic currents through the scale. In this scenario oxygen is thus cathodically reduced at the scale surface. It is argued that in the present case the reduction of alkali chromate provides an alternative cathodic process:

$$K_2CrO_4(s) + 3e^- + H_2O(g) \rightleftarrows 2KOH(l) + {}^1\!/_2Cr_2O_3(s) \tag{6}$$

The cathodic current is provided by metal oxidation:

$$Fe(s) \rightleftarrows Fe^{2+} + 2e^- \tag{7}$$

$$Cr(s) \rightleftarrows Cr^{3+} + 3e^- \tag{8}$$

The potassium hydroxide formed in this way can either react with the surface oxide or be volatilized [24]:

$$\begin{aligned} &2KOH(l) + Fe_2O_3(s) \rightleftarrows K_2Fe_2O_4(s) + H_2O(g) \\ &\Delta G = -44.7\,\text{kJ at } 600\,^{\circ}\text{C} \end{aligned} \tag{9}$$

$$\begin{aligned} &KOH(l) \rightleftarrows KOH(g) \\ &\Delta G = 72\,\text{kJ}, \quad p_{eq}(KOH(g)) = 4.9 \times 10^{-5}\,\text{bar at } 600\,^{\circ}\text{C} \end{aligned} \tag{10}$$

Because of its high equilibrium vapour pressure, KOH is not likely to be present in pure form at 600 °C.

Considering its similarity to K_2CrO_4 it is expected that Na_2CrO_4 would decompose in a similar way (i.e. forming NaOH):

$$Na_2CrO_4(s) + 3e^- + H_2O(g) \rightleftarrows 2NaOH(l) + {}^1\!/_2Cr_2O_3(s) \tag{11}$$

However, the results show that the amount of sodium chromate does not decrease with time as in the case of potassium chromate. Another significant difference between the effects of KCl and NaCl is that while the amount of K^+ corresponds to the number of moles of chromate and chloride detected, the amount of Na^+ exceeds the number of moles of chromate and chloride found, suggesting alkaline condition on the surface. The disparity between Na and chromate + chlorine was confirmed by EDX point analysis. It is suggested that these differences are explained by the

lower volatility of NaOH compared to KOH. Thus, the equilibrium vapour pressure over the corresponding pure condensed phase at 600 °C is 5.3×10^{-7} and 4.9×10^{-5} bar for NaOH and KOH respectively. This means that while the decomposition of K_2CrO_4 produces KOH, which is easily vaporized, the NaOH formed by decomposition of Na_2CrO_4 is expected to accumulate on the surface, in accordance with our observations. The alkaline environment created in this way is suggested to slow down the decomposition of Na_2CrO_4 (11).

The sodium hydroxide accumulated on the surface may react with iron oxide, forming sodium ferrate(III) [24]:

$$\begin{aligned} &2NaOH(l) + Fe_2O_3(s) \rightleftarrows Na_2Fe_2O_4(s) + H_2O(g) \\ &\Delta G = -61\,\text{kJ at } 600\,^\circ\text{C} \end{aligned} \tag{12}$$

Alkali ferrate(III) may also form by reaction of the applied salt with hematite [24]:

$$\begin{aligned} &2NaCl(s) + Fe_2O_3(s) + H_2O(g) \rightleftarrows Na_2Fe_2O_4(s) + 2HCl(g) \\ &\Delta G = 191\,\text{kJ/mol}, \quad p(HCl) = 1.2 \times 10^{-6}\,\text{bar at } 600\,^\circ\text{C}, 40\,\%H_2O \end{aligned} \tag{13}$$

$$\begin{aligned} &2KCl(s) + Fe_2O_3(s) + H_2O(g) \rightleftarrows K_2Fe_2O_4(s) + 2HCl(g) \\ &\Delta G = 260\,\text{kJ/mol}, \quad p(HCl) = 1.03 \times 10^{-8}\,\text{bar at } 600\,^\circ\text{C}, 40\,\%H_2O \end{aligned} \tag{14}$$

It may be noted that the formation of sodium ferrate is much more favoured compared to potassium ferrate. It is therefore suggested that the greater stability of sodium chromate in comparison to potassium chromate can be attributed to the more alkaline conditions that prevail on the NaCl-treated samples.

In spite of these differences regarding corrosion chemistry, it is important to note that the corrosion effect of NaCl and KCl are generally speaking quite similar in these conditions.

In contrast to NaCl and KCl, $CaCl_2$ is only slightly corrosive under the exposure conditions. One explanation is that $CaCl_2$ is readily converted to CaO [24]:

$$\begin{aligned} &2CaCl_2 + H_2O \rightleftarrows CaO + 2HCl(g) \\ &\Delta G = 119\,\text{kJ}, \quad pHCl = 169 \times 10^{-6}\,\text{bar at } 600\,^\circ\text{C}, 40\,\%H_2O. \end{aligned} \tag{15}$$

Accordingly, the quantitative analysis of the samples after oxidation (Table 4) show that only 12 % of the added chloride remains on the surface after 1 h of oxidation. This indicates that most of the $CaCl_2$ has been converted to CaO at this stage. However, XRD analysis gave only weak diffraction from CaO while no evidence was found for $CaCl_2$ or its hydrates. The thermal decomposition of $CaCl_2$ to CaO is known to proceed through intermediate steps and several calcium-hydroxychlorides and -oxychlorides have been described (e.g. Ca(OH)Cl) [18]. These compounds are metastable and tend to be poorly crystalline. Thus, the chloride remaining on the surface after 1 h of exposure is mainly attributed to calcium-hydroxychlorides and –oxychlorides. After 24 h only 2 % of the added chloride remains. At this stage there is strong diffraction from CaO and $Ca_2Fe_2O_5$. The latter compound corresponds to the iron- and calcium-rich band seen in Fig. 10, encircling a former $CaCl_2$ agglomeration. Apparently, reaction (15) is now completed and parts of the CaO

formed has reacted further with iron oxide at the scale/gas interface (reaction 16) [24].

$$\begin{aligned} &Fe_2O_3(s) + 2CaO(s) \rightleftarrows Ca_2Fe_2O_5(s) \\ &\Delta G = -63\,\text{kJ/mol at } 600\,^{\circ}\text{C} \end{aligned} \tag{16}$$

Because of its rapid thermal decomposition, $CaCl_2$ does not have the opportunity to react extensively with the chromium-rich oxide as is the case for NaCl and KCl. However, small amounts of calcium chromate are detected around the former $CaCl_2$ agglomerates (reaction 17).

$$\begin{aligned} &Cr_2O_3(s) + 2CaCl_2(s) + 2H_2O(g) + {}^3\!/_2O_2(g) \rightleftarrows 2CaCrO_4(s) + 4HCl(g) \\ &\Delta G = 127\,\text{kJ/mol}, \quad p\text{HCl} : 2602 \times 10^{-6}\,\text{bar at } 600\,^{\circ}\text{C}, 5\,\%O_2, 40\,\%H_2O \end{aligned} \tag{17}$$

Calcium chromate can also form by reaction with CaO (reaction 18). Because of the poor mobility of CaO, Ca does not spread over the surface and the reaction between Ca and the protective oxide is limited [24].

$$\begin{aligned} &Cr_2O_3(s) + CaO(s) + {}^3\!/_2O_2(g) \rightleftarrows 2CaCrO_4(s) \\ &\Delta G = -112\,\text{kJ/mol at } 600\,^{\circ}\text{C}, 5\,\%O_2 \end{aligned} \tag{18}$$

Because of the small extent of chromate formation, the protective oxide is not chromium depleted in a major way, explaining why exposure in the presence of $CaCl_2$ does not result in accelerated corrosion, compared to the reference exposure, in the absence of salt. Accordingly, the oxidation morphology is similar to that observed in 5 $\%O_2$ + 40 $\%H_2O$ environment in the absence of salt [23]. Thus, Fig. 13 shows a two-layered oxide consisting of an outer iron-rich part and an inner layer that contains iron, chromium and nickel. In the area previously covered by $CaCl_2$, three scale layers can be detected. The outer part is rich in Fe and Ca (corresponding to $Ca_2Fe_2O_5$). The middle and bottom parts correspond to the scale formed away from the salt agglomeration. Thus, the middle part is iron-rich together with small amounts of chromium (probably corresponding to Fe_2O_3) while the inner part contains iron, chromium and nickel (spinel oxide, $(Fe, Cr, Ni)_3O_4$). Noticeable is that the bottom spinel oxide layer is thinner than the corresponding oxide formed adjacent to the former salt agglomerate. This may indicate that the top $Ca_2Fe_2O_5$ layer acts as a barrier. The slightly lower mass gain of the $CaCl_2$ exposed samples compared to the salt free exposures is not considered to be significant because of the occurrence of substantial scale spallation at the location of the former $CaCl_2$ agglomerations (see Fig. 4). Spallation is also suggested to explain why the Ca^{2+} content decreases with time, see Table 4. In addition, the thermal decomposition of $CaCl_2$ forming CaO and HCl(g) also contributes to a lower mass gain. All the chlorine added corresponds to 0.09 mg/cm^2.

Figure 13 also shows two small areas enriched in chlorine at the metal/oxide interface. This corresponds to sub-scale transition metal chlorides formed by the alloy. It is suggested that the small amounts of chloride detected by IC analysis can be attributed to such sub-scale chlorides. It appears that the chloride accumulations do not influence corrosion in a major way in the present case.

Conclusions

The presence of KCl and NaCl strongly accelerates the high temperature corrosion of 304L stainless steel in 5 $\%O_2$ + 40 $\%H_2O$ environment. The corrosion is initiated by the formation of alkali chromate(VI) through the reaction of alkali with the protective oxide. Chromate formation is a sink for chromium in the oxide and leads to a loss of its protective properties. Subsequently a rapidly growing scale forms, consisting of an outer hematite layer with chromate particles on top and an inner layer consisting of spinel oxide, $(Fe, Cr, Ni)_3O_4$. While the extent of corrosion attack is similar for samples exposed to NaCl and KCl, some differences are observed. Thus, the amount of Na_2CrO_4 formed was higher compared to K_2CrO_4, the latter compound decomposing with time. Furthermore, the samples exposed in the presence of NaCl formed a corrosion product containing Na, Fe and O, possibly $Na_2Fe_2O_4$. In contrast, the only alkali-containing product forming on the KCl-treated samples was K_2CrO_4. These differences are attributed to the greater volatility of KOH compared to NaOH.

In contrast to NaCl and KCl, $CaCl_2$ is not very corrosive. Under the exposure conditions $CaCl_2$ is rapidly converted to CaO. Because of the poor mobility of CaO, only small amounts of $CaCrO_4$ form where CaO is in direct contact with the scale. CaO also reacts with the scale to form $Ca_2Fe_2O_5$.

Acknowledgment This work was carried out within the High Temperature Corrosion Centre (HTC) at Chalmers University of Technology.

References

1. K. O. Davidsson, L. E. Amand, B. Leckner, B. Kovacevik, M. Svane, M. Hagstrom, J. B. C. Pettersson, J. Pettersson, H. Asteman, J. E. Svensson, and L. G. Johansson, *Energy & Fuels* **21**, 71 (2007).
2. J. Pettersson, C. Pettersson, N. Folkeson, L.-G. Johansson, E. Skog, and J.-E. Svensson, *Materials Science Forum* **522–523**, 563 (2006).
3. H. P. Nielsen, F. J. Frandsen, K. Dam-Johansen, and L. L. Baxter, *Progress in Energy and Combustion Science* **26**, 283 (2000).
4. N. Folkeson, J. Pettersson, C. Pettersson, L. G. Johansson, E. Skog, B. Å. Andersson, S. Enestam, J. Tuiremo, A. Jonasson, B. Heikne, and J. E. Svensson, *Materials Science Forum* **595–598**, 289 (2008).
5. H. P. Michelsen, F. Frandsen, K. Dam-Johansen, and O. H. Larsen, *Fuel Processing Technology* **54**, 95 (1998).
6. H. J. Grabke, E. Reese, and M. Spiegel, *Corrosion Science* **37**, 1023 (1995).
7. M. Montgomery and A. Karlsson, *Materials and Corrosion* **50**, 579 (1999).
8. H. P. Nielsen, F. J. Frandsen, and K. Dam-Johansen, *Energy & Fuels* **13**, 1114 (1999).
9. C. J. Wang and T. T. He, *Oxidation of Metals* **58**, 415 (2002).
10. M. Montgomery, A. Karlsson, and O. H. Larsen, *Materials and Corrosion* **53**, 121 (2002).
11. N. Folkeson, T. Jonsson, M. Halvarsson, L.-G. Johansson, and J.-E. Svensson, *Materials and Corrosion* (2010). doi:10.1002/maco.201005942.

12. C. Pettersson, L. G. Johansson, and J. E. Svensson, *Oxidation of Metals* **70**, 241 (2008).
13. C. Pettersson, J. Pettersson, H. Asteman, J. E. Svensson, and L. G. Johansson, *Corrosion Science* **48**, 1368 (2006).
14. J. Pettersson, H. Asteman, J.-E. Svensson, and L.-G. Johansson, *Oxidation of Metals* **64**, 23 (2005).
15. C. Proff, T. J., C. Pettersson, J.-E. Svensson, L.-G. Johansson, and M. Halvarsson, Submitted to *Microscopy of Oxidation* (2008).
16. T. Jonsson, et al., *Oxidation of Metals* **72**, 213 (2009).
17. J. Pettersson, N. Folkeson, J.-E. Svensson, and L.-G. Johansson, *Oxidation of Metals* **76**(1–2), 93 (2011).
18. L. Gmelin, *Gmelins Handbuch der anorganischen Chemie* (1924–1997).
19. H. Asteman, J. E. Svensson, L. G. Johansson, and M. Norell, *Oxidation of Metals* **52**, 95 (1999).
20. H. Asteman, J. E. Svensson, M. Norell, and L. G. Johansson, *Oxidation of Metals* **54**, 11 (2000).
21. J. E. Tang, et al., *Micron* **32**, 799 (2001).
22. B. Pujilaksono, T. Jonsson, M. Halvarsson, I. Panas, J.-E. Svensson, and L.-G. Johansson, *Oxidation of Metals* **70**, 163 (2008).
23. M. Halvarsson, J. E. Tang, H. Asteman, J.-E. Svensson, and L.-G. Johansson, *Corrosion Science* **48**, 2014 (2006).
24. I. Barin, *Thermodynamic Data of Pure Substances*, 3rd edn. (1995).